Bioconjugate Chemistry

Article

Cite This: *Bioconjugate Chem.* 2019, 30, 2614−2623

pubs.acs.org/bc

Construction of Anti-hPD-L1 HCAb Nb6 and *in Situ* ^{124}I Labeling for Noninvasive Detection of PD-L1 Expression in Human Bone Sarcoma

Hai-Feng Huang,[†,‡,#] Hua Zhu,[§,#] Guang-Hui Li,[∥,#] Quan Xie,[†] Xian-Teng Yang,[†,‡] Xiao-Xia Xu,[§] Xiao-Bin Tian,[*,⊥] Ya-Kun Wan,[*,∥] and Zhi Yang[*,§]

[†]Guizhou University School of Medicine, Guizhou University, Guiyang 550025, Guizhou, P. R. China

[‡]Department of Orthopedics, Guizhou Provincial People's Hospital, Guiyang 550002, Guizhou, P. R. China

[§]Key Laboratory of Carcinogenesis and Translational Research (Ministry of Education/Beijing), Department of Nuclear Medicine, Peking University Cancer Hospital & Institute, Beijing 100142, P. R. China

[∥]Shanghai Novamab Biopharmaceuticals Co., Ltd., Shanghai 201203, P. R. China

[⊥]Clinical Medical College of Guizhou Medical University, Guiyang 550025, Guizhou, P. R. China

Supporting Information

ABSTRACT: Immunotherapy is considered the fourth major treatment mode for cancer following surgery, chemotherapy, and radiotherapy. In recent years, tumor immunotherapy has achieved breakthrough progress; therefore, it is important to screen patients to identify those who will respond to tumor immunotherapy. Here, we report the construction of a novel heavy chain-only antibody (HCAb) and its corresponding ^{124}I-labeled probe. Using phage display technology, we generated a novel anti-hPD-L1-specific HCAb named Nb6 (selected from 95 monoclones) with high affinity for hPD-L1. The positron-emitting ^{124}I-labeled hPD-L1-targeted HCAb probe was prepared for further evaluation, and nonradioactive natural iodine (^{nat}I)-labeled anti-hPD-L1 Nb6 was synthesized as a reference compound. ^{125}I-anti-hPD-L1 Nb6 uptake in OS-732 cells *in vitro* can be blocked by the precursor. The binding affinity of ^{125}I-anti-hPD-L1 Nb6 to OS-732 cell lines was 2.19 nM. For *in vivo* studies, an osteosarcoma OS-732 tumor-bearing mouse model was successfully constructed. Polymerase chain reaction (PCR) and Western blot analyses were performed to confirm the presence of the hPD-L1 gene and antigen in the tumor tissue of the OS-732 mouse model. Biodistribution showed that uptake of ^{124}I-anti-hPD-L1 Nb6 probes at 24 h was 4.43 ± 0.33% ID/g in OS-732 tumor tissues. Tumor lesions can be clearly delineated on micro-PET (positron emission tomography)/CT (computed tomography) imaging 24 h after injection of ^{124}I-anti-hPD-L1 Nb6, while the blocking group shows substantially decreased uptake on imaging. Pathological staining validated hPD-L1 expression on the surface of the tumor cell membrane; thus, ^{124}I-anti-hPD-L1 Nb6 can be used for *in vivo* noninvasive PET imaging. When administered in tandem, Nb6 and ^{124}I-anti-hPD-L1 Nb6 may provide a novel strategy to clinically screen patients for hPD-L1 to identify those who would benefit from immunotherapy of malignant tumors such as osteosarcoma.

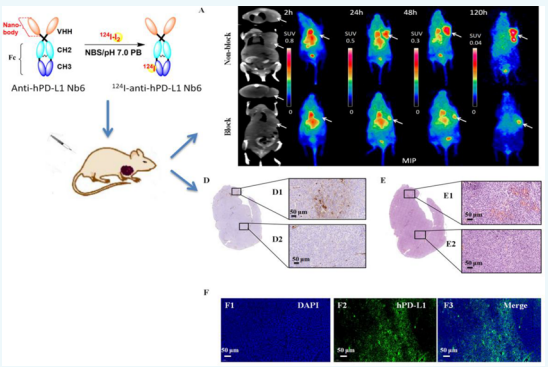

INTRODUCTION

PD-1/PD-L1 (programmed cell death-1/programmed cell death ligand-1) drugs specifically act on T cells and enhance the immune killing function of the body's activated T cells, which has helped achieve breakthrough effects in the treatment of cancer.[1] With the development of oncology, immunology, and imaging studies, immunotherapy has become another important method for treating tumors following traditional therapies (chemotherapy, surgical resection, and radiation therapy). Blocking the PD-1/PD-L1 signaling pathway may be used for the treatment of advanced solid tumors, and cancer immunotherapy is predicted to become a vital part of the clinical treatment of cancer.[2] The overall efficacy rate of monoclonal antibodies that target the PD-1/PD-L1 pathway in different patients is 20−40%; however, in patients positive for PD-1/PD-L1 expression, monoclonal antibody treatment may be up to 90% effective.[3−5] Sundara et al.[6] identified positive PD-L1 expression in 13% of primary osteosarcomas, 25% of relapsed osteosarcomas, and 48% of osteosarcoma metastases, and this expression was correlated with high T cell infiltration (p = 0.002). Compared with primary osteosarcoma, metastases had an increased number of tumor-infiltrating T cells and PD-L1 expression. Osteosarcoma is the most common primary malignant bone tumor. One study indicated that the 1-, 2-, and 5-year survival rates of osteosarcoma patients with lung metastases are 93.3%, 61.5%, and 11.5%, respectively.[7] Soft-

Received: August 10, 2019
Revised: September 16, 2019
Published: September 19, 2019

DOI: 10.1021/acs.bioconjchem.9b00539
Bioconjugate Chem. 2019, 30, 2614−2623

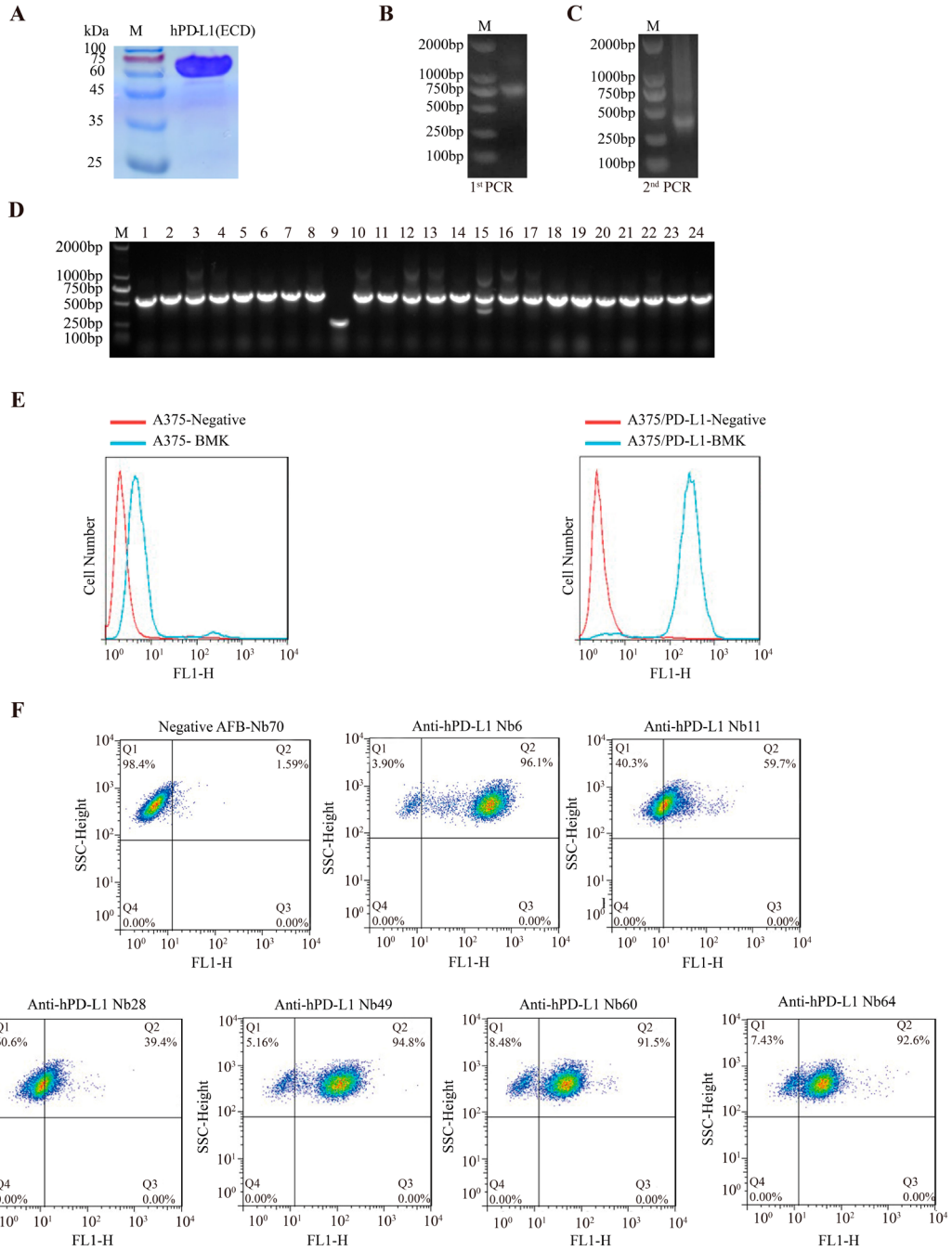

Figure 1. Generation of high-affinity hPD-L1-specific HCAbs. (A) Expressed and purified hPD-L1 was detected by SDS-PAGE. (B) Fragments containing VHH genes were first amplified by PCR, with an initial band of approximately 700 bp. (C) Fragments were amplified by a second PCR, with a band of approximately 400 bp. (D) Determination of the insertion rate of the anti-hPD-L1 library by PCR amplification. (E) FACS analysis of the established cell line with stable hPD-L1 overexpression. (F) Screening of the affinity of the constructed HCAbs to A375/hPD-L1 using transfected cells by FACS.

tissue sarcomas (STSs) are a group of aggressive, heterogeneous, and rare tumors with relatively few efficient systemic therapies and a high metastatic risk. PD-L1 expression is also a poor prognostic factor in STS.[8] Blocking the PD-1/PD-L1 interaction in patients with osteosarcoma should be used as a therapeutic strategy. Therefore, it is important to screen for patients expressing PD-1/PD-L1 based on relevant literature.

The expression level of PD-1/PD-L1 in patients is positively correlated with the treatment response and negatively correlated with the prognosis; thus, anti-PD-L1 monoclonal antibodies could reverse the immune checkpoint and release the blockade of the T cell response.[9] Immune checkpoint inhibitors for the treatment of cancer are a revolutionary innovation in oncology.[10] PD-L1 is a transmembrane protein highly expressed on the membrane of cancer cells.[11] Immunotherapies, particularly with checkpoint inhibitors, such as anti-PD-L1 and anti-PD-1 antibodies, have changed the prognosis of melanoma and the standard of care.[12] It is well established that many tumors use checkpoint systems to evade antitumor immune responses.[13] PD-L1 expression is a poor prognostic factor, and immunohistochemistry (IHC) staining indicates that PD-L1 is present on the membranes of both

DOI: 10.1021/acs.bioconjchem.9b00539
Bioconjugate Chem. 2019, 30, 2614−2623

immune cells and tumor cells.[14] Research confirms that PD-L1 overexpression predicts activity and correlates with better survival for individuals treated with immune checkpoint inhibitors.[15]

These excellent characteristics of PD-L1 make it extremely suitable for use in noninvasive molecular imaging. In 2015, a study by Heskamp et al. showed the feasibility of noninvasive *in vivo* imaging with ^{111}In-PD-L1.3.1 to detect PD-L1 expression in tumors.[16] Josefsson et al. developed ^{111}In-diethylenetriaminepentaacetic acid (DTPA)-anti-PD-L1, which binds to antibodies, to study breast cancer in mouse models.[17]

However, in the clinical setting, the sensitivity, quantification, and resolution of single-photon emission computerized tomography (SPECT) are inferior to those of positron emission tomography (PET). A recent study has shown the results of the first human imaging study with ^{89}Zr-labeled anti-PD-L1.[18] Here, we report the generation of the novel PD-L1-targeting heavy chain-only antibody (HCAb) Nb6 and *in situ* ^{124}I-labeled Nb6 for evaluating the hPD-L1 status by micro-PET/CT in an osteosarcoma mouse model. The combination of HCAb Nb6 and ^{124}I-labeled Nb6 may provide a novel strategy for guiding patient selection for hPD-L1 immunotherapy of malignant tumors such as osteosarcoma.

RESULTS

Construction of the hPD-L1 Immune Phage Display Library and Screening and Identification of anti-hPD-L1 HCAb. The immune library was chosen for anti-hPD-L1 HCAb generation in this study due to its advantages compared to the nonimmune library and synthetic library, such as its higher affinity and specificity. The extracellular domain (ECD) of the hPD-L1 antigen was produced by a mammalian expression system and identified by SDS-PAGE to assess the quality of the antigen hPD-L1(ECD). The results showed that we obtained hPD-L1(ECD) with high quality (Figure 1A).

Immunization with hPD-L1(ECD) was then performed weekly seven times, and peripheral blood was collected after the last injection and processed for RNA extraction. RNA was subsequently transcribed to cDNA, and the variable domain of the heavy chain of heavy chain-only antibody (VHH) genes were amplified by nested polymerase chain reaction (PCR). As shown in Figure 1B, the first PCR fragments have evident bands at approximately 700 bp. As demonstrated in Figure 1C, the 400 bp bands correspond to the VHH-only region enriched from the first PCR products, which served as templates via nested PCR. The VHH fragments were then ligated into the pMECS[19] vector and transformed into TG1 *E. coli* cells. The cells were then cultured to generate the VHH library. The library size and insertion rate were subsequently measured, and the library size was estimated to be approximately 3×10^8 colony-forming units (CFUs). The insertion rate of the immune library against hPD-L1(ECD) was 95.8% (Figure 1D), which was evaluated by PCR in the 24 randomly selected colonies. Overall, we successfully constructed a high-quality phage display library against hPD-L1(ECD). The detailed procedures of biopanning can be referenced in our previous study.[20] We performed three rounds of screening for hPD-L1(ECD), as shown in Figure S1A. After three rounds of biopanning, the relative enrichment increased to 14-fold in the second round and 171-fold in the third round. Next, 95 HCAb clones were randomly selected to identify the positive colonies against hPD-L1(ECD) by periplasmic extraction enzyme-linked immunosorbent assay (PE-ELISA). Ultimately, 30 of 95 colonies were identified as positive colonies, and the plasmids of these 30 colonies were extracted and sequenced. Based on the amino acid sequences and the removed repeated sequences, there were only six remaining colonies with unique sequences. We then subcloned these six plasmids into a mammalian expression vector containing an Fc label for flow-activated cell sorting (FACS).

Establishment of a Cell Line with Stable hPD-L1 Overexpression. PD-L1 is a protein expressed on the plasma membrane, and we used human A375 cells to establish a cell line stably overexpressing hPD-L1 to screen hPD-L1-specific HCAbs. A375 cells were stably transfected with hPD-L1, and the successful clones were determined by calibrated flow cytometry. As shown in Figure 1E, the fluorescence intensity of the hPD-L1 benchmark antibody (blue line, obtained from the IMGT Web site: http://imgt.org/3Dstructure-DB/cgi/details.cgi?pdbcode=9814) clearly shifted, which indicated that the cell surface expression levels of hPD-L1 sharply increased. This signified that we successfully constructed an A375 cell line that stably overexpressed hPD-L1 on the cell membrane.

Screening of High Binding Affinity HCAbs to hPD-L1 Using Transfected Cells by FACS. The six previously described anti-hPD-L1 HCAbs with unique sequences were produced in a mammalian expression system and tagged with Fc tag such that FITC-labeled goat anti-human Fc antibodies could be used to analyze the affinity of the HCAbs to the A375 stable cell line. Parental A375 cells served as the negative strain, and Aflatoxin B1-specific HCAb AFB-Nb70-Fc was used as an isotype control. As illustrated in Figure 1F, flow cytometric dot plots showed the binding activity of anti-hPD-L1 HCAbs to A375/hPD-L1 cells, which was indicated by the fluorescence intensity of the HCAbs-Fc-FITC staining. Compared with the cells treated with the negative isotope AFB-Nb70-Fc, the majority of cells treated with the anti-hPD-L1 HCAbs exhibited an increased fluorescence intensity, which indicates that all six HCAbs can bind to hPD-L1 proteins on the A375/hPD-L1 cell membrane. In particular, HCAb Nb6 had the highest fluorescence intensity; thus, Nb6 had the best binding activity of hPD-L1 and was used for subsequent experiments.

Measurement of the Binding Affinity of Monovalent HCAb Nb6. To confirm the binding affinity of hPD-L1-Fc-specific HCAb, we conducted an affinity measurement of monovalent anti-hPD-L1 HCAb Nb6 derived from in *E. coli* WK6 cells. First, the quality of monovalent HCAb Nb6 was identified by sodium dodecyl sulfate polyacrylamide gel electrophoresis (SDS-PAGE) (shown in Figure S1B); the molecular weight of monovalent HCAb Nb6 was approximately 15 kDa, which was equal to the theoretical value. The purity was ≥90%, which was satisfactory to perform the affinity measurement. The binding affinity of monovalent HCAb Nb6 containing a 6×His tag with recombinant hPD-L1-Fc protein was subsequently assessed by a ForteBio Octet RED96 System assay.[21,22] As monovalent HCAb Nb6 was immobilized, hPD-L1-Fc was added at six concentrations (0.625, 1.25, 2.5, 5, 10, and 20 nM). All data were fitted to a 1:1 interaction model, the simplest model for the description of the interaction between an antigen and a monovalent antibody. The binding affinity results in Figure S1C indicate that monovalent HCAb Nb6 showed high affinity and strong binding to hPD-L1 with an equilibrium dissociation constant (K_D) of 1.23×10^{-9} M (k_a of 1.23×10^6 M^{-1} s^{-1} and k_d of 1.51×10^{-3} s^{-1}); all details of the

DOI: 10.1021/acs.bioconjchem.9b00539
Bioconjugate Chem. 2019, 30, 2614−2623

monovalent HCAb Nb6 affinity measurements are provided in Table S1.

Estimation of the Biochemical Characteristics of Humanized HCAb Nb6. Because HCAb Nb6 was developed for human therapeutics, it is required that the antibody undergoes a humanization process. According to the published humanization principles, we modified the HCAb Nb6 by mutating key sites of the nucleotide sequence,[23] synthetizing the sequences into the pFUSE-hIgG1-Fc vector and expressing them in a mammalian expression system. The biochemical characteristics of the best humanization candidate were estimated by performing affinity measurements using the ForteBio Octet RED96 System assay, and the inhibition of PD-1/PD-L1 binding was assessed by FACS.

The information is presented in Figure S2A,B; antigen hPD-L1 with no tag was immobilized, and HCAb Nb6-Fc and humanized HCAb Nb6-Fc were measured at concentrations of 0.625, 1.25, 2.5, 5, 10, and 20 nM. For the binding affinity of HCAb Nb6-Fc, as Figure S2A indicates, HCAb Nb6-Fc showed high affinity and strong binding to hPD-L1 with an equilibrium dissociation constant (K_D) of 1.84×10^{-9} M (k_a of 3.49×10^6 M^{-1} s^{-1} and k_d of 6.43×10^{-3} s^{-1}); additional information regarding HCAb Nb6-Fc is provided in Table S2. Furthermore, the binding affinity of humanized HCAb Nb6-Fc is shown in Figure S2B with a K_D of 1.84×10^{-9} M (k_a of 3.24×10^6 M^{-1} s^{-1} and k_d of 5.97×10^{-3} s^{-1}); the results showed that the binding affinity did not change after humanization. These data indicate that we have successfully created humanized HCAb-Nb6 with high binding affinity to hPD-L1.

The blocking activity between PD-1 and PD-L1 of humanized HCAb-Nb6 was also identified with AFB-Nb70 as the negative control. The hPD-L1-overexpressing stable cell line and hPD-1-Fc protein were used in this assay. As Figure S2C demonstrates, the half-maximal inhibitory concentration (IC_{50}) value of humanized HCAb-Nb6 (8.82 nM) was greater than that of untreated HCAb-Nb6 (6.79 nM). The results showed that humanization slightly affected the blocking activity of humanized HCAb Nb6 compared to HCAb Nb6. Therefore, we conclude that the humanization of HCAb-Nb6 altered the blocking ability between PD-1 and PD-L1, whereas the binding activity had no effect. Therefore, the humanized HCAb Nb6 we constructed had good binding activity of hPD-L1 and was equipped with good blocking activity of PD-1 and PD-L1, and was thus suitable in subsequent experiments.

Quality Control and Stability of ^{124}I-anti-hPD-L1 Nb6. A schematic diagram of the ^{124}I-labeled hPD-L1 Nb6 probe is shown in Figure S3. The quality control data of ^{124}I-anti-hPD-L1 Nb6 is shown in Table S4. As shown in Figure S4, free ^{124}I was not found in the final product ^{124}I-anti-hPD-L1 Nb6 by radio-TLC. Radio-HPLC showed that the radioactive peak retention time of ^{124}I-anti-hPD-L1 Nb6 was 7.02 min and the UV peak retention time of ^{124}I-anti-hPD-L1 Nb6 was 6.55 min. The radiochemical purification yield was greater than 97% in 5% HSA and was greater than 93% in phosphate buffered solution (PBS) after 48 h at 37 °C (Figure S5). After purification, the specific activity was 45 KBq/μmol.

^{nat}I-anti-hPD-L1 Nb6 Activity Assay. The average molecular weight of anti-hPD-L1 Nb6 before iodine modification as measured by MALDI-TOF-MS was 77 857 Da (Figure 2A). After modification with ^{nat}I, the average molecular weight of ^{nat}I-anti-hPD-L1 Nb6 was 79 204 Da (Figure 2B). Therefore, the average molecular weight of the HCAbs changed by approximately 10 ^{nat}I linkages. ELISA was used to detect the binding ability of HCAbs before and after iodine modification. The optical density (OD) value of the sample was subtracted from the OD value of the blank control, as well as the ordinate, and a four-parameter pseudocooperative map was established (Figure 2C). The half-maximal effective concentration (EC_{50}) value of the modified HCAb before and after ^{nat}I modification was 0.65 ± 0.08 ng/mL and 0.70 ± 0.09 ng/mL, respectively. There was no significant difference between the EC_{50} values (Figure 2D) ($t = -1.13$, $P > 0.05$).

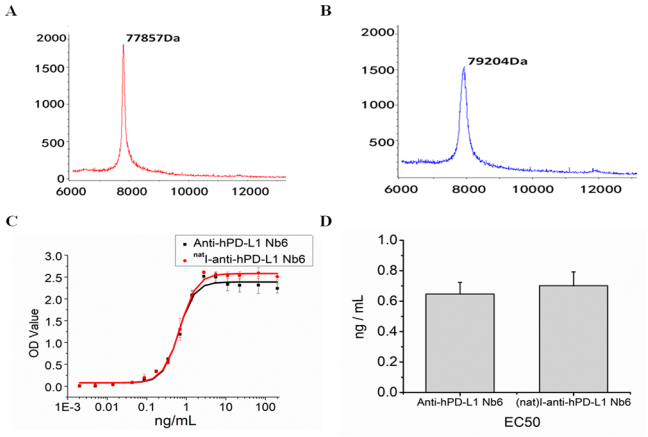

Figure 2. Characterization of ^{nat}I-anti-hPD-L1 Nb6. (A) Average molecular weight of anti-hPD-L1 Nb6 as measured by MALDI-TOF-MS before iodine modification (77 857 Da). (B) Average molecular weight of ^{nat}I-anti-hPD-L1 Nb6 measured by MALDI-TOF-MS after ^{nat}I modification (79 204 Da). (C) Comparison of the binding ability of anti-hPD-L1 Nb6 to the hPD-L1 receptor before and after ^{nat}I modification. (D) There was no significant change in the EC_{50} values of anti-hPD-L1 Nb6 and ^{nat}I-anti-hPD-L1 Nb6 ($P > 0.05$).

***In Vitro* Experiments.** The expression of hPD-L1 in OS-732 cells was identified by immunofluorescence (IF) (Figure 3A–C) and flow cytometry (Figure S7). The cellular uptake of ^{125}I-anti-hPD-L1 Nb6 in OS-732 cells (%IA/CC 10^6 cells, %IA/CC: percent of collected count of total added count per milliliter) from 10 to 120 min gradually increased. After cells

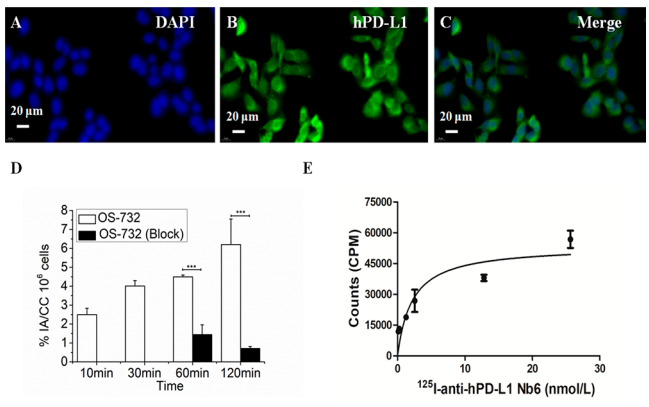

Figure 3. (A) DAPI staining of the nuclei of OS-732 cells. (B) hPD-L1 staining of OS-732 cells. (C) Merged image of nuclear and hPD-L1 staining. (D) Radioactivity uptake of ^{125}I-anti-hPD-L1 Nb6 in OS-732 cells (%IA/CC 10^6 cells). The radioactivity uptake of ^{125}I-anti-hPD-L1 Nb6 in OS-732 cells was significantly reduced at 60 and 120 min after blocking. ***$P < 0.001$. (E) Affinity of ^{125}I-anti-hPD-L1 Nb6 in OS-732 cells; the K_d value was 2.19 nM.

DOI: 10.1021/acs.bioconjchem.9b00539
Bioconjugate Chem. 2019, 30, 2614–2623

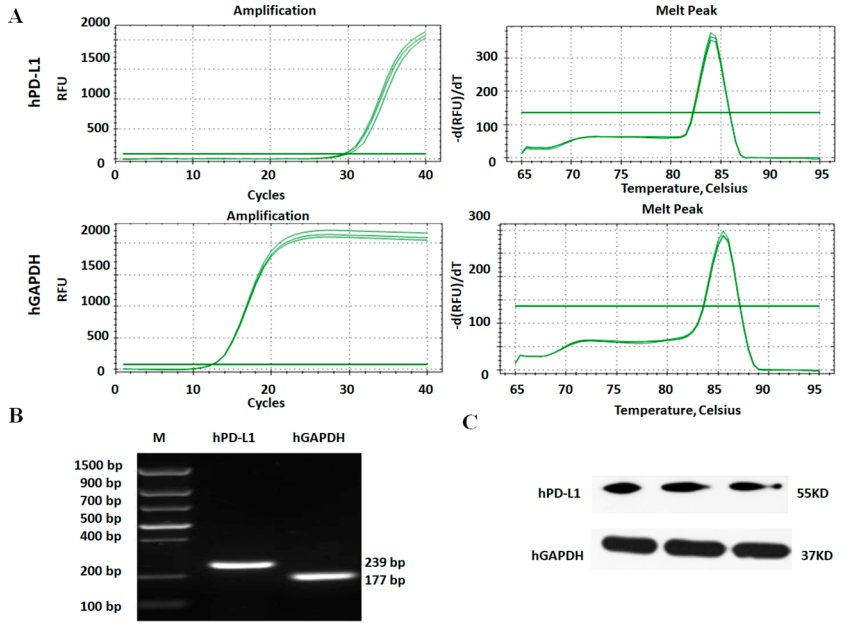

Figure 4. Identification of hPD-L1 in tumor tissues. (A) Inflection point of the hPD-L1 and hGAPDH gene amplification curves was clear, the baseline levels were basic, the recurrence rate of the CT value was high, and the index period was clear. (B) Gel electrophoresis results show that the amplified product conforms to the hPD-L1 target gene fragment size, which was 239 bp, and that the amplification product was specific. (C) Protein expression of the hPD-L1 receptor was positive in tumor tissues; human GAPDH was used as an internal control protein.

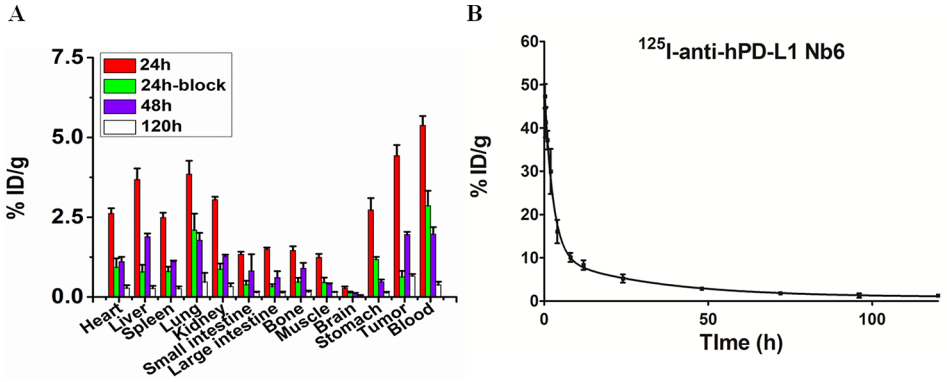

Figure 5. Biodistribution and metabolism of $^{124/125}$I-anti-hPD-L1 Nb6. (A) Biodistribution of ^{124}I-anti-hPD-L1 Nb6 in the heart, liver, spleen, lung, kidneys, small/large intestine (with contents), bone, muscle, brain, stomach (with contents), tumor, and blood of tumor-bearing mice at 24, 48, and 120 h after injection (The 24-h-block group was coinjected with 500 μg of anti-hPD-L1 Nb6). (B) Metabolism of ^{125}I-anti-hPD-L1 Nb6 probes in KM mouse blood was measured at each time point after injection.

were blocked with anti-hPD-L1 Nb6, the value of the uptake was significantly reduced at 60 min (4.49 ± 0.10 vs 1.45 ± 0.51, $P < 0.001$) and 120 min (6.20 ± 1.35 vs 0.71 ± 0.10, $P < 0.001$) (Figure 3D). These results suggest that ^{125}I-anti-hPD-L1 Nb6 had a specific targeting ability for hPD-L1 expressed on tumor cells. Based on the OS-732 cell binding affinity determination, the K_d value reached 2.19 nM (Figure 3E).

PCR and Western Blot Analysis of Human PD-L1 Expression. Quantitative PCR was performed on the tumor tissue, and the hPD-L1 gene was further amplified and separated by gel electrophoresis. The results showed that the target gene hPD-L1 was expressed (Figure 4A) and matched the calculated hPD-L1 gene fragment size (Figure 4B). The Cq value of the hPD-L1 gene was 30.67 ± 0.4, and that of the human GAPDH gene was 12.43 ± 0.06. After the PCR amplification product was sequenced, the DNA sequence was compared to the NCBI database. The results showed that the PCR product was the hPD-L1 gene. Western blot analysis of the tumor tissue specimens was performed and indicated that hPD-L1 protein expression was present in the tumor tissues (Figure 4C).

Biodistribution and Metabolism Analysis of $^{124/125}$I-anti-hPD-L1 Nb6. The biodistribution of ^{124}I-anti-hPD-L1 Nb6 in tumor-bearing mice was evaluated at 24 and 48 h (Figure 5A). The uptake of ^{124}I-anti-hPD-L1 Nb6 in tumor tissue was 4.43 ± 0.33% ID/g at 24 h and 1.96 ± 0.08% ID/g at 48 h. The tumor/blood (T/B) values at 24 and 48 h were 0.83 ± 0.06 and 1.01 ± 0.12, respectively, while the tumor/muscle (T/M) values at 24 and 48 h were 3.61 ± 0.54 and 4.85 ± 0.37, respectively. As shown in Figure 5B, ^{125}I-anti-hPD-L1 Nb6 exhibited a similar blood distribution in KM mice (5.22 ± 0.97% ID/g, and 2.88 ± 0.29% ID/g) to that of ^{124}I-anti-hPD-L1 Nb6 in tumor-bearing mice (5.38 ± 0.29% ID/g, and 1.97 ± 0.22% ID/g) at 24 and 48 h after injection. The metabolism of ^{125}I-labeled probes (0.555 MBq, 100 μL/each mouse) in KM mouse blood fit the two-compartment model.

DOI: 10.1021/acs.bioconjchem.9b00539
Bioconjugate Chem. 2019, 30, 2614−2623

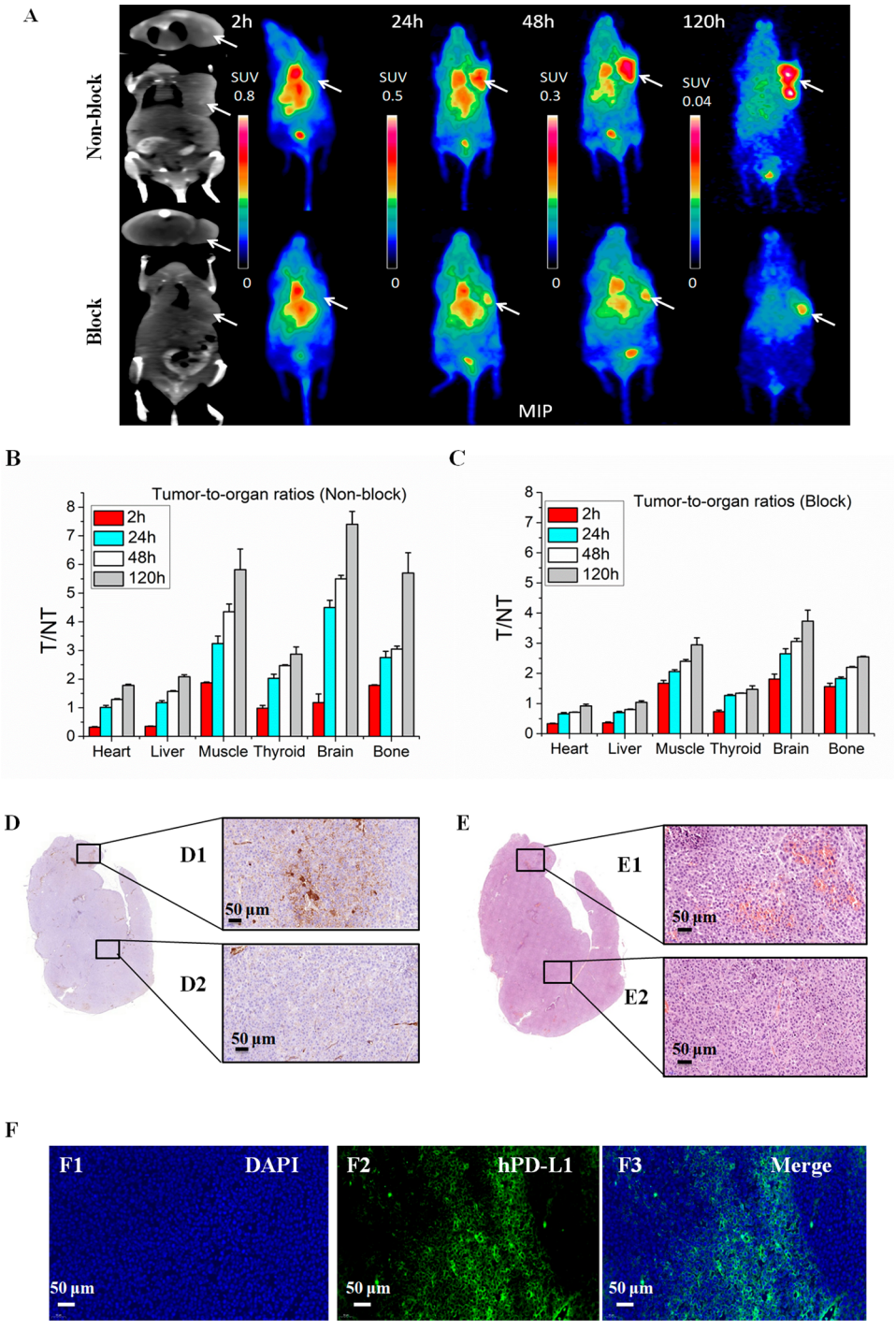

Figure 6. ^{124}I-anti-hPD-L1 Nb6 tumor uptake and pathological staining (white arrow indicates tumor). (A) Micro-PET imaging at each time point after injection of 18.5 MBq ^{124}I-anti-hPD-L1 Nb6 or coinjection of 18.5 MBq ^{124}I-anti-hPD-L1 Nb6 and 500 μg of anti-hPD-L1 Nb6. (B) T/NT SUV_{mean} ratios at each time point after injection of the probes in the nonblocking group. (C) T/NT SUV_{mean} ratios at each time point after coinjection of ^{124}I-anti-hPD-L1 Nb6 probes and 500 μg anti-hPD-L1 Nb6 in the blocking group. (D) IHC staining of hPD-L1 receptors in tumor tissues in the high and low hPD-L1 expression regions. (E) HE staining of hPD-L1 receptors in tumor tissues in the high and low hPD-L1 expression regions. (F1) DAPI staining image of the nuclei in OS-732 tumors. (F2) hPD-L1 staining in OS-732 tumors. (F3) Merged image of nuclear and hPD-L1 staining in OS-732 tumors.

Micro-PET/CT Imaging. For imaging, 18.5 MBq ^{124}I-anti-hPD-L1 Nb6 was injected via tail vein and circulated for 2 h; there was no obvious uptake at the tumor site based on imaging. The probes mainly clustered in the heart and liver of nude mice (Figure 6A). When micro-PET/CT imaging was performed 24 h after injection, apparent uptake was observed at the tumor site. At 120 h after injection, the residual probes in the liver were basically metabolized. In the blocking group, micro-PET/CT imaging was performed at 2, 24, 48, and 120 h after coinjection of 18.5 MBq ^{124}I-anti-hPD-L1 Nb6 and 500 μg anti-hPD-L1 Nb6, and the uptake at the tumor site of the blocking group was less than that in the nonblocking group. The SUV_{mean} ratios of T/NT in both the blocking and

DOI: 10.1021/acs.bioconjchem.9b00539
Bioconjugate Chem. 2019, 30, 2614−2623

nonblocking groups gradually increased with time (Figure 6B,C).

IHC, IF, and HE Staining. IHC (Figure 6D) and IF staining (Figure 6F) of tumor tissue in the nonblocking groups indicated that hPD-L1 protein was expressed on the surface of the tumor cell membrane. Hematoxylin and eosin (HE) staining showed that the OS-732 human osteosarcoma cells had no organizational form, the arrangement of the tumor cells was irregular, and the heterogeneity of the nucleus was obvious (Figure 6E).

DISCUSSION

Imaging of PD-L1 is a hot topic, with several studies recently reporting on this field.[24,25] Immunotarget-related imaging mainly includes SPECT, PET, optical imaging, and MRI. Each imaging method has its own inherent advantages and disadvantages in indicating tumor morphology and physiology. In this study, we used phage display technology to generate an anti-hPDL1-specific HCAb named Nb6, which was selected from 95 monoclones, with a high affinity for hPD-L1. Under the guidance of clear, high-quality images, the best results can be achieved after drug treatment. Our work shows that Nb6 exhibits substantial binding affinity to PD-L1, the combination of anti-hPD-L1 Nb6 and ^{124}I labeling is novel, and ^{124}I-anti-hPD-L1 Nb6 can be used for *in vivo* noninvasive PET imaging.

In recent years, studies on ^{111}In-, ^{64}Cu-, and ^{89}Zr-labeled PD-L1 imaging probes have been reported, in which a labeled PD-L1 monoclonal antibody has been used in clinical studies and has shown good imaging results.[16−18,26,27] However, ^{111}In can only be imaged with SPECT, while the half-life of ^{64}Cu (approximately 12.7 h) is relatively short compared to that of ^{124}I (approximately 4.2 days). ^{89}Zr shows a similar half-life to that of ^{124}I, and both are suitable for antibody evaluation. However, owing to the lack of bifunctional chelators (currently, only DFO is commercially available), critical labeling conditions, long incubation times, and, in some cases, antibody aggregation make ^{89}Zr difficult to use. The ^{124}I labeling method is *in situ* labeling, it does not require bifunctional chelators, and the labeling is simple and convenient. Moreover, the average molecular weight of Nb6 (about 78 kDa) in this study is half that of the general antibody (150 kDa), and it also has potential advantages in the tissue penetrating ability and metabolic rate *in vivo*. The visual observation of the PD-L1 receptor in this study is extended as long as 120 h after injection. According to Figure 5A, tumor and blood activities seem to be similar at later time points (48 h after the injection); there may be a possibility of blood pool activity of antibodies contributing to tumor activity. Consistent with the literature,[28] ^{124}I-labeled probe uptake in the thyroid can be blocked by ^{nat}I, which can avoid the toxicity of ^{124}I to the thyroid gland. The expression of hPD-L1 in OS-732 cells was observed by IF staining. *In vitro*, uptake of radioactive probes by tumor cells can be blocked by the precursor. The binding affinity of ^{125}I-anti-hPD-L1 Nb6to OS-732 cell lines was high, up to 2.19 nM.

In this study, we labeled HCAb with ^{nat}I and determined the changes in the HCAb EC50 values. The HCAb Nb6 we prepared did not show a significant decrease in activity after ^{nat}I labeling, which may be related to the good stability of the HCAb Nb6 and our construction method, which may not interfere as much with the active group of HCAbs. The average molecular weight of HCAbs increased 1347 Da after the reaction (corresponding to approximately 10 ^{nat}I linkages), and this increase in mass did not significantly change the affinity of the anti-hPD-L1 Nb6; therefore, it is predicted that the radioactive ^{124}I label will not change the Nb6 affinity.

We verified the expression of PD-L1 in OS-732 tumor tissues by PCR and Western blot and prepared models for further imaging experiments. Twenty-four hours after injection of the ^{124}I-anti-hPD-L1 Nb6 probes, the tumor site showed good imaging, and the probes could be specifically blocked by the PD-L1 HCAb.

Traditional methods for detecting PD-L1 expression in tumor tissues, such as IHC or Western blot, are invasive. In addition, there is a risk of seeding iatrogenic tumors when tumor specimens are obtained. Kim et al.[29] confirmed the presence of PD-L1 in tumors, whereas PD-1 is mainly expressed in tumor-infiltrating lymphocytes. The goal of most immunotherapies is the activation of immune effectors, such as T cells and natural killer cells. However, immune checkpoint inhibitors (such as PD-1, PD-L1, and cytotoxic T lymphocyte antigen 4 (CTLA4)) inhibit the function of T cells and promote immune evasion. Nivolumab is an anti-PD-1/PD-L1 checkpoint inhibitor; however, only 15−24% of patients are likely to respond. To date, there are no validated biomarkers, including PD-L1 expression, that can accurately identify patients who are likely to respond to immune checkpoint therapy.[30] Anti-PD-L1 treatment is beneficial only for certain patients. PD-1/PD-L1 suppresses antitumor immunity; thus, blocking PD-L1 in clinical settings may lead to dramatic responses in a subset of patients.[31] Patients who derive benefit from immune-based therapies tend to have better progression-free survival (PFS) in response to conventional therapies following administration of an anti-PD-L1 agent.[32] The anti-hPD-L1 HCAb described in this study is a humanized HCAb that blocks the activity of PD-L1 and PD-1. Noninvasive imaging of PD-L1 is very meaningful, because immunotherapy is more effective in PD-L1-positive patients, and identifying a tumor with potential PD-L1 expression can further assist in the diagnosis and treatment.

Moreover, this study provides a new probe for the noninvasive screening of PD-L1 in patients through nuclear medicine technology. This technology is expected to increase the response rate of patients to PD-L1 HCAb treatment. This study would lay the foundation for our further study, in which a humanized mouse model will be used to mimic the clinical situation and verify whether the HCAb Nb6 was suitable to develop with PET-CT for diagnosis and clinical fields.

CONCLUSION

This study shows that a novel hPD-L1 HCAb named Nb6 has high affinity to hPD-L1. The $^{124/125}$I-labeled hPD-L1-targeting HCAb probe was prepared and confirmed to specifically target hPD-L1. The ^{124}I-labeled probe targeted the hPD-L1 receptor on the surface of human bone sarcoma cell membranes and was successfully imaged by PET/CT up to 120 h after probe injection. Both Nb6 and the ^{124}I-anti-hPD-L1 Nb6 probe may become important tools for the implementation of immunotherapy in malignant tumors, including osteosarcoma.

METHODS

Materials and Reagents. The coding sequence of human PD-L1 (hPD-L1) was achieved from the UniProt Web site (https://www.uniprot.org/). The hPD-L1 extracellular domain

DOI: 10.1021/acs.bioconjchem.9b00539
Bioconjugate Chem. 2019, 30, 2614−2623

(ECD) was prepared by our laboratory with human embryonic kidney (HEK) 293F cells. Freund's complete adjuvant, Freund's incomplete adjuvant, anti-mouse IgG-alkaline phosphatase, ampicillin, isopropyl β-D-1-thiogalactopyranoside (IPTG), and bovine serum albumin (BSA) were purchased from Sigma-Aldrich (USA). Mouse anti-HA antibody was obtained from Covance (USA). Lymphocyte isolation sterile solution was provided by GE Healthcare (USA). Oligo (dT) primer and fluorescein isothiocyanate (FITC) were purchased from Thermo Scientific (USA). *Pst*I and *Not* I were obtained from NEB (USA). Ninety-six-well plates were purchased from Thermo Scientific NUNC (Denmark). VCSM13 helper phages (Filamentous phage), TG1 cells, and WK6 cells were obtained from Prof. Serge Muyldermans (Laboratory of Cellular and Molecular Immunology, Vrije Universiteit Brussel, Belgium). FITC-labeled goat anti-human Fc antibody was supplied by Abcam (UK). The isotopes $^{124}I-I_2$ and $Na^{125}I$ were obtained from the Department of Nuclear Medicine, Peking University Cancer Hospital. Refer to the Supporting Information for additional content.

Generation of anti-PD-L1(ECD) HCAbs. Phage display technology was used for HCAb generation as previously described.[33] Briefly, hPD-L1(ECD) was manufactured via HEK 293F cells, linked to an Fc tag after purification and identification by sodium dodecyl sulfate polyacrylamide gel electrophoresis (SDS-PAGE). A two-year-old male Bactrian camel was immunized with high-quality hPD-L1(ECD)-Fc antigen at a dose of 1 mg per injection. The hPD-L1(ECD)-Fc antigen was diluted in PBS (137 mM NaCl, 10 mM phosphate, and 2.7 mM KCl), and equal volumes of Freund's complete adjuvant (first time) and Freund's incomplete adjuvant (following six times) were then added and ground with a pestle until the component appeared milky white and was difficult to disperse. The injections were conducted every week for a total of seven injections. Peripheral blood from the camel was collected after the final immunization. After total RNA was extracted and reverse-transcribed to cDNA, the variable domain of the heavy chain of heavy chain-only antibody (VHH) genes was amplified by two-step nested PCR. After the PCR products were digested with *Pst*I and *Not* I, the VHH fragments (approximately 400 bp) and the pMECS phagemid vector were electrotransformed into *Escherichia coli (E. coli)* TG1 cells. The transformants were subsequently cultured, and a library quality evaluation was performed.

Generation of A375 Cells Stably Transfected with Human PD-L1. The A375 cell line was obtained from the Chinese Academy of Sciences Cell Bank of Type Culture Collection and maintained in DMEM supplemented with 10% FBS and penicillin/streptomycin. A375 cells were stably transfected with pLVX-hPD-L1 plasmid encoding the sequence for full-length hPD-L1 by lipofection with Lipofectamine 2000 reagent according to the standard operating protocol. Forty-eight hours post-transfection, cells were exposed to 2 μg/mL puromycin for selection. The cell pool was ultimately harvested and authenticated by flow cytometry using hPD-1-Fc and FITC-labeled goat anti-human Fc antibodies to detect the hPD-L1 expression level of the constructed stable cells.

Construction and Expression of Fc Fusion HCAb Nb6. HCAb Nb6 was designed to construct into pFUSE-hIgG1-Fc vector, according to the nucleotide sequence of HCAb Nb6 and the vector; the PCR primers were synthesized to amplify the gene of HCAb Nb6. After purification of the PCR products, the homologous recombination strategy was utilized to clone HCAb Nb6 directly into pFUSE-hIgG1-Fc vector. Afterward, the recombinant plasmid was sequenced and transfected into *E. coli* cells assuming the aligned results were correct. At last, the plasmid HCAb Nb6-Fc fusion protein was expressed via HEK 293F cells.

Natural Iodine (^{nat}I)-anti-hPD-L1 Nb6 Affinity. After 200 μL of phosphate buffer (PB; 0.1 M, pH 7.0) was added to 1 mg of anti-hPD-L1 Nb6 (5 mg/mL, 200 μL), a KI (potassium iodide) solution with a molar ratio 100 times the excess was added. Then, 25 μL of NBS (*N*-bromosuccinimide, 1 mg/mL, pH 7.0) was added to the reaction system for 60 s, after which the solution was subject to purification. The average molecular masses of anti-hPD-L1 Nb6 before and after ^{nat}I modification were measured by MALDI-TOF-MS. The EC_{50} values of anti-hPD-L1 Nb6 and ^{nat}I-anti-hPD-L1 Nb6 were tested by ELISA, and other details are described in the Supporting Information.

Radiochemical Stability. ^{124}I-anti-hPD-L1 Nb6 (100 μL, 3.7 MBq) was incubated under shaking conditions at 37 °C in a thermomixer. The stability of ^{124}I-anti-hPD-L1Nb6 in 0.1 M PBS (pH = 7.0) and in 5% HSA was measured by radio-TLC. The time points included 2, 24, and 48 h.

***In Vitro* Experiment.** OS-732 cells were provided by the Institute of Cancer in Chinese Academy of Medical Sciences and cultured in a humidified incubator at 37 °C with 5% CO_2. hPD-L1 expression in OS-732 cells was measured using immunofluorescence (IF) staining and flow cytometry analysis. Details are provided in the Supporting Information.

Cell Uptake Experiment. Approximately 3×10^5 OS-732 cells per well were seeded into a 24-well plate, with 4 wells per group. The experimental group was divided into groups 1, 2, 3, and 4, while the competitive inhibition group was divided into groups 5 and 6. In the competitive inhibition group, 20 μg of the anti-hPD-L1 Nb6 was added for 2 h, and 37 KBq ^{125}I-anti-hPD-L1 Nb6 was subsequently added to each well for incubation. Groups 1, 2, 3, and 4 were sampled at 10, 30, 60, and 120 min, respectively. Groups 5 and 6 were incubated for 60 and 120 min, respectively. The cells were washed twice with 1 mL of PBS. Adherent cells were detached from the well surface with 0.5 M NaOH 1 mL, and the radioactivity counts were measured.

K_d Value Measurement. Approximately 3×10^5 OS-732 cells per well were seeded into a 24-well plate, with 6 groups of 4 wells. Different concentrations of ^{125}I-anti-hPD-L1 Nb6 (1.85 KBq, 3.7 KBq, 18.5 KBq, 37 KBq, 185 KBq, and 370 KBq) in 20 μL of PBS were added to each well. After incubation for 240 min, the radioactivity counts were measured.

Mouse Model. Human OS-732 cells (2×10^6/each) were harvested in the logarithmic growth phase, and normal BALB/c nude mice (Beijing Huafukang Bioscience Co. Ltd.) were inoculated in the right axilla and fed under SPF conditions. After the tumor diameter reached approximately 1.0 cm, the relevant experimental *in vivo* study was performed.

All procedures performed in studies involving animals were conducted in accordance with the ethical standards of the institutional and/or national research committee and the 1964 Helsinki Declaration and its later amendments or comparable ethical standards.

Human PD-L1 PCR and Western Blot Assay. After the tumor tissue was extracted, total RNA was reverse-transcribed to cDNA, which was then subjected to PCR (polymerase chain

DOI: 10.1021/acs.bioconjchem.9b00539
Bioconjugate Chem. 2019, 30, 2614−2623

reaction). The primers used were as follows: GAPDH, upstream 5′-CAAGAGCACAAGAGGAAGAGAGAGA-3′, downstream 5′-GGTTGAGCACAGGGTACTTTATTGA-3′; and hPD-L1, upstream 5′-CCTGGCGAAAGCAGAGGA-GGA-3′, downstream 5′-GCATTGAGTGGAGGCAAAGGG-CA-3′. The expression of hPD-L1 in the OS-732 tumor tissue was measured using Western blot. Other details are described in the Supporting Information.

Biodistribution and Metabolic Analysis of $^{124/125}$I-anti-hPD-L1 Nb6. Three days prior to injection of radiopharmaceuticals, the thyroid gland was blocked by providing a 5‰ KI solution to the mice. Biodistribution studies were performed by tail vein injection of 1.11 MBq ^{124}I-anti-hPD-L1 Nb6 radiotracer in OS-732 tumor-bearing mice (n = 4). Healthy KM mice (n = 6) were selected for the time−radioactivity concentration curve. At 15 min, 30 min, 1 h, 2 h, 4 h, 8 h, 12 h, 24 h, 48 h, 72 h, 96 h, and 120 h after 555 KBq ^{125}I-anti-hPD-L1 Nb6 injection, 50 μL of blood was collected from each mouse. The organs of interest were collected at 120 h and weighed, and the radioactivity was counted with a γ-counter. Data are calculated as the percentage of injected dose per gram of blood/organ by comparison with a 1:100 diluted standard dose (%ID/g).

Micro-PET Imaging. Three days prior to injection of the radiopharmaceuticals, the thyroid gland was blocked by feeding 5‰ KI solution to human OS-732 tumor-bearing mice. Then, 18.5 MBq ^{124}I-anti-hPD-L1 Nb6 was injected into each tumor-bearing mouse via tail vein. The control group was coinjected with 500 μg (100 μL, 5 mg/mL) of anti-hPD-L1 Nb6 and 18.5 MBq ^{124}I-anti-hPD-L1 Nb6. At each different time point (2, 24, 48, and 120 h) after injection, the mice were anesthetized with 1.5% isoflurane and placed near the center of the field of the PET scanner (Sedecal, Spain); 10 min static scans were subsequently obtained. A two-dimensional ordered subset expectation maximum algorithm was employed to reconstruct the images. The regions of interest (ROIs) of the radiotracer in each organ were sketched to estimate the uptake.

Pathological Analysis. OS-732 tumor-bearing mice were sacrificed after imaging. IF and immunohistochemistry (IHC) analyses were performed to confirm the expression of hPD-L1 on the surface of the OS-732 tumor cell membranes. HE staining was performed to show the morphology of the OS-732 tumor tissue. Other details are described in the Supporting Information.

Statistical Analysis. Statistical analysis was performed with the SPSS software package (v 17.0; SPSS, Chicago, IL, USA). The t test was used to analyze differences in the data. $P < 0.05$ was considered statistically significant.

■ ASSOCIATED CONTENT

Supporting Information

The Supporting Information is available free of charge on the ACS Publications website at DOI: 10.1021/acs.bioconjchem.9b00539.

General materials and methods; radiosynthesis of ^{124}I-anti-hPD-L1 Nb6; characterization of the compounds; flow cytometry and IF staining of cells; pathological analysis, ELISA, PCR, and Western blot assay; binding activity of HCAb Nb6 (PDF)

■ AUTHOR INFORMATION

Corresponding Authors

*E-mail: txb6@vip.163.com (X.B.T.).
*E-mail: ykwan@novamab.com (Y.K.W.).
*E-mail: pekyz@163.com (Z.Y.).

ORCID

Zhi Yang: 0000-0003-2084-5193

Author Contributions

#H.F.H., H.Z., and G.H.L. contributed equally to this work.

Notes

The authors declare no competing financial interest.

■ ACKNOWLEDGMENTS

This work is funded by the National Natural Science Foundation of China (No. 31471216, 81673344, 81560356, 81571705, and 81671733), the Beijing Nova Program (Z171100001117020), Beijing Excellent Talents Funding (2017000021223ZK33), the Beijing Municipal Administration of Hospitals-Yangfan Project (ZYLX201816), the Beijing Natural Science Foundation, Jing-Jin-Ji special projects for basic research cooperation (H2018206600), and the Science and Technology Foundation of Guizhou Province (No. gzwjkj2018-1-040, and No. (2019)1201)). The funding bodies had no role in the study design, data collection and analysis, decision to publish, or preparation of the manuscript.

■ REFERENCES

(1) Postow, M. A., Callahan, M. K., and Wolchok, J. D. (2015) Immune Checkpoint Blockade in Cancer Therapy. *J. Clin. Oncol. 33*, 1974−1982.

(2) Wang, X., Huang, S., Zhang, Y., Zhu, L., and Wu, X. (2018) The application and mechanism of PD pathway blockade for cancer therapy. *Postgrad. Med. J. 94*, 53−60.

(3) Ohaegbulam, K. C., Assal, A., Lazar-Molnar, E., Yao, Y., and Zang, X. (2015) Human cancer immunotherapy with antibodies to the PD-1 and PD-L1 pathway. *Trends Mol. Med. 21*, 24−33.

(4) Gibney, G. T., Weiner, L. M., and Atkins, M. B. (2016) Predictive biomarkers for checkpoint inhibitor-based immunotherapy. *Lancet Oncol. 17*, No. e542.

(5) Wang, X., Teng, F., Kong, L., and Yu, J. (2016) PD-L1 expression in human cancers and its association with clinical outcomes. *OncoTargets Ther. 9*, 5023−5039.

(6) Sundara, Y. T., Kostine, M., Cleven, A. H., Bovée, J. V., Schilham, M. W., and Cleton-Jansen, A. M. (2017) Increased PD-L1 and T-cell infiltration in the presence of HLA class I expression in metastatic high-grade osteosarcoma: a rationale for T-cell-based immunotherapy. *Cancer Immunol. Immunother. 66*, 119−128.

(7) Ren, J., Xu, Y. F., Kuang, T. H., Chen, J., and Liu, Y. X. (2017) Survival analysis of 104 cases of osteosarcoma with lung metastases. *Zhonghua Zhong Liu Za Zhi 39*, 263−268.

(8) Bertucci, F., Finetti, P., Perrot, D., Leroux, A., Collin, F., Le Cesne, A., Coindre, J. M., Blay, J. Y., Birnbaum, D., and Mamessier, E. (2017) PDL1 expression is a poor-prognosis factor in soft-tissue sarcomas. *Oncoimmunology 6*, No. e1278100.

(9) Hu, B., Jacobs, R., and Ghosh, N. (2018) Checkpoint Inhibitors Hodgkin Lymphoma and Non-Hodgkin Lymphoma. *Curr. Hematol. Malig. Rep. 13*, 543−554.

(10) Arasanz, H., Gato-Cañas, M., Zuazo, M., Ibañez-Vea, M., Breckpot, K., Kochan, G., and Escors, D. (2017) PD1 signal transduction pathways in T cells. *Oncotarget 8*, 51936−51945.

(11) Kalim, M., Chen, J., Wang, S., Lin, C., Ullah, S., Liang, K., Ding, Q., Chen, S., and Zhan, J. (2017) Construction of high level prokaryotic expression and purification system of PD-L1 extracellular domain by using Escherichia coli host cell machinery. *Immunol. Lett. 190*, 34−41.

DOI: 10.1021/acs.bioconjchem.9b00539
Bioconjugate Chem. 2019, 30, 2614−2623

(12) Sivade, A., Bensaid, D., Monnier, Y., Shabafrouz, K., Bouchaab, H., and Cristina, V. (2017) Head and neck cancer: promising results of immunotherapy. *Rev. Med. Suisse 13*, 1029−1031.
(13) Dal Bello, M. G., Alama, A., Coco, S., Vanni, I., and Grossi, F. (2017) Understanding the checkpoint blockade in lung cancer immunotherapy. *Drug Discovery Today 22*, 1266−1273.
(14) Mann, S. A., Lopez-Beltran, A., Massari, F., Pili, R., Fiorentino, M., Koch, M. O., Kaimakliotis, H. Z., Wang, L., Scarpelli, M., Ciccarese, C., Moch, H., Montironi, R., and Cheng, L. (2017) Targeting the Programmed Cell Death-1 Pathway in Genitourinary Tumors: Current Progress and Future Perspectives. *Curr. Drug Metab. 18*, 700−711.
(15) Aguiar, P. N., Jr., De Mello, R. A., Hall, P., Tadokoro, H., and Lima Lopes, G. (2017) PD-L1 expression as a predictive biomarker in advanced non-small-cell lung cancer: updated survival data. *Immunotherapy 9*, 499−506.
(16) Heskamp, S., Hobo, W., Molkenboer-Kuenen, J. D., Olive, D., Oyen, W. J., Dolstra, H., and Boerman, O. C. (2015) Noninvasive Imaging of Tumor PD-L1 Expression Using Radiolabeled Anti-PD-L1 Antibodies. *Cancer Res. 75*, 2928−2936.
(17) Josefsson, A., Nedrow, J. R., Park, S., Banerjee, S. R., Rittenbach, A., Jammes, F., Tsui, B., and Sgouros, G. (2016) Imaging, Biodistribution, and Dosimetry of Radionuclide-Labeled PD-L1 Antibody in an Immunocompetent Mouse Model of Breast Cancer. *Cancer Res. 76*, 472−479.
(18) Bensch, F., van der Veen, E. L., Lub-De Hooge, M. N., Jorritsma-Smit, A., Boellaard, R., Kok, I. C., Oosting, S. F., Schröder, C. P., Hiltermann, T. J. N., van der Wekken, A. J., Groen, H. J. M., Kwee, T. C., Elias, S. G., Gietema, J. A., Bohorquez, S. S., de Crespigny, A., Williams, S. P., Mancao, C., Brouwers, A. H., Fine, B. M., and de Vries, E. G. E. (2018) ^{89}Zr-atezolizumab imaging as a non-invasive approach to assess clinical response to PD-L1 blockade in cancer. *Nat. Med. 24*, 1852−1858.
(19) Vincke, C., Gutiérrez, C., Wernery, U., Devoogdt, N., Hassanzadeh-Ghassabeh, G., and Muyldermans, S. (2012) Generation of single domain antibody fragments derived from camelids and generation of manifold constructs. *Methods Mol. Biol. 907*, 145−176.
(20) Pan, D., Li, G., Hu, H., Xue, H., Zhang, M., Zhu, M., Gong, X., Zhang, Y., Wan, Y., and Shen, Y. (2018) Direct Immunoassay for Facile and Sensitive Detection of Small Molecule Aflatoxin B1 based on Nanobody. *Chem. - Eur. J. 24*, 9869−9876.
(21) Xu, H., Wang, Y., Chen, Y., Zhang, P., Zhao, Y., Huang, Y., Wang, X., and Sheng, J. (2016) Subcellular Localization of Galloylated Catechins in Tea Plants [Camellia sinensis (L.) O. Kuntze] Assessed via Immunohistochemistry. *Front Plant Sci. 7*, 728.
(22) Vasylieva, N., Kitamura, S., Dong, J., Barnych, B., Hvorecny, K. L., Madden, D. R., Gee, S. J., Wolan, D. W., Morisseau, C., and Hammock, B. D. (2019) Nanobody-based binding assay for the discovery of potent inhibitors of CFTR inhibitory factor (Cif). *Anal. Chim. Acta 1057*, 106−113.
(23) Vincke, C., Loris, R., Saerens, D., Martinez-Rodriguez, S., Muyldermans, S., and Conrath, K. (2009) General strategy to humanize a camelid single-domain antibody and identification of a universal humanized nanobody scaffold. *J. Biol. Chem. 284*, 3273−3284.
(24) Broos, K., Lecocq, Q., Raes, G., Devoogdt, N., Keyaerts, M., and Breckpot, K. (2018) Noninvasive imaging of the PD-1:PD-L1 immune checkpoint: Embracing nuclear medicine for the benefit of personalized immunotherapy. *Theranostics 8*, 3559−3570.
(25) Du, Y., Jin, Y., Sun, W., Fang, J., Zheng, J., and Tian, J. (2019) Advances in molecular imaging of immune checkpoint targets in malignancies:current and future prospect. *Eur. Radiol. 29*, 4294−4302.
(26) Lesniak, W. G., Chatterjee, S., Gabrielson, M., Lisok, A., Wharram, B., Pomper, M. G., and Nimmagadda, S. (2016) PD-L1 Detection in Tumors Using [(64)Cu]Atezolizumab with PET. *Bioconjugate Chem. 27*, 2103−2110.
(27) Hettich, M., Braun, F., Bartholomä, M. D., Schirmbeck, R., and Niedermann, G. (2016) High-Resolution PET Imaging with Therapeutic Antibody-based PD-1/PD-L1 Checkpoint Tracers. *Theranostics 6*, 1629−1640.
(28) Wang, F., Liu, T., Li, L., Guo, X., Duan, D., Liu, Z., Zhu, H., and Yang, Z. (2018) Production, quality control of next-generation PET radioisotope iodine-124 and its thyroid imaging. *J. Radioanal. Nucl. Chem. 318*, 1999.
(29) Kim, J. R., Moon, Y. J., Kwon, K. S., Bae, J. S., Wagle, S., Kim, K. M., Park, H. S., Lee, H., Moon, W. S., Chung, M. J., Kang, M. J., and Kang, K. Y. (2013) Tumor infiltrating PD1-positive lymphocytes and the expression of PD-L1 predict poor prognosis of soft tissue sarcomas. *PLoS One 8*, No. e82870.
(30) Teo, M. Y., and Rosenberg, J. E. (2018) Nivolumab for the treatment of urothelial cancers. *Expert Rev. Anticancer Ther. 18*, 215−221.
(31) Munn, D. H. (2018) The host protecting the tumor from the host-targeting PD-L1 expressed by host cells. *J. Clin. Invest. 128*, 570−572.
(32) Aspeslagh, S., Matias, M., Palomar, V., Dercle, L., Lanoy, E., Soria, J. C., and Postel-Vinay, S. (2017) In the immuno-oncology era, is anti-PD-1 or anti-PD-L1 immunotherapy modifying the sensitivity to conventional cancer therapies? *Eur. J. Cancer 87*, 65−74.
(33) Li, G., Zhu, M., Ma, L., Yan, J., Lu, X., Shen, Y., and Wan, Y. (2016) Generation of Small Single Domain Nanobody Binders for Sensitive Detection of Testosterone by Electrochemical Impedance Spectroscopy. *ACS Appl. Mater. Interfaces 8*, 13830−13839.

DOI: 10.1021/acs.bioconjchem.9b00539
Bioconjugate Chem. 2019, 30, 2614−2623